Applied Energy 311 (2022) 118608

Contents lists available at ScienceDirect

Applied Energy

journal homepage: www.elsevier.com/locate/apenergy

On the dynamics of a model wind turbine under passive tower oscillations

Buen Zhang [a,b], Yaqing Jin [c], Shyuan Cheng [b], Yuan Zheng [d], Leonardo P. Chamorro [b,e,f,g,*]

[a] China Renewable Energy Engineering Institute, Beijing, 100120, China
[b] Department of Mechanical Science and Engineering, University of Illinois, Urbana, IL, 61801, United States of America
[c] Department of Mechanical Engineering, The University of Texas at Dallas, Richardson, TX, 75080, United States of America
[d] College of Water Conservancy and Hydropower Engineering, Hohai University, Nanjing 210024, China
[e] Department of Aerospace Engineering, University of Illinois, Urbana, IL, 61801, United States of America
[f] Department of Civil and Environmental Engineering, University of Illinois, Urbana, IL, 61801, United States of America
[g] Department Geology, University of Illinois, Urbana, IL, 61801, United States of America

ARTICLE INFO

Keywords:
Small-amplitude oscillations
Turbine wake
Yawing
Power output fluctuations
Passive motions

ABSTRACT

Laboratory experiments were carried out to quantify the effect of small-amplitude, passive oscillations of a model wind turbine in the structure of the unsteady motions, wake statistics, and mean power output and associated fluctuations at various yawing $\beta \in [0^o,\ 30^o]$ every $\Delta\ \beta = 5^o$. Planar particle image velocimetry was used to characterize the flow statistics, and power output was measured at high temporal resolution. Scenarios with a fixed turbine were included to aid insight into the coupled and separated effects of passive oscillations and yawing. Unsteady pitch motions, dominant of the system dynamics, were more predominant at small but non-zero yaw of $\beta \approx 5^o$. The spectral structure of the oscillations showed that the unsteady roll motions contributed substantially under high yawing. Using basic concepts, we derived a formulation for the turbine oscillation spectrum that shows good agreement with measurements; it serves as a base to include other input modulation types. The power output decreased monotonically with β in the fixed and oscillating turbines, which was more distinct for $\beta > 15^o$. Passive oscillations produced higher power for given yaw. A simple yaw-correction of the structure of the power output also showed reasonable agreement with measurements. Finally, mean velocity in the wake of the fixed and oscillating turbines exhibited minor differences for a given yawing. However, the turbulence levels showed distinct changes of turbine motions in the degree of symmetry and magnitude for given yaw.

1. Introduction

Wind energy plays an essential role in the global energy portfolio; it is one of the most promising technologies [1]. Wind turbines have been experiencing a monotonic increase in size and power capacity, with trends pointing toward offshore floating settings [2,3], notably, in deep-sea conditions characterized by comparatively higher and more consistent winds [4,5]. Given that advantageous land-based wind energy is becoming scarce, offshore offers vast possibilities with enormous energy potential [6]. However, it brings numerous engineering challenges that are not well understood.

Quantification of the loads and unsteady forcing on floating turbines is crucial in the systems' engineering design and life span. The coupled wind-wave forcing on floating wind turbines may result in excessive translational (heave, sway, and surge) and rotational (yaw, pitch, and roll) motions [7]. Control strategies have been of particular interest in floating platforms to mitigate oscillations [8–10] in complex environmental conditions [11,12]. Bayati, Belloli, Ferrari, Fossati, and Giberti [13] used a six-degrees-of-freedom platform for studying floating-like turbines in a wind-tunnel environment; they discussed kinematic and dynamic aspects of architectures. Recent numerical efforts have focused on aerodynamic characteristics of floating offshore wind turbines (FOWTs) under simple motions, including, for instance, surge and pitch [14–18]. The effects of multiple motions on the dynamic response and wake characteristics of the FOWTs is also receiving attention [19,20]. Still, the unsteady aerodynamics and loads on FOWTs are open, complex problems.

Various studies have shown that the unsteady loads on turbine blades are substantially modulated by the frequency and amplitude of platform motions [21–24]. Surge motion, in particular, can contribute to widening the range of aerodynamics force, power output, and flow field around the rotor of offshore floating wind turbines [25–28]. Numerical simulations on the unsteady aerodynamics of turbine–platform systems considering pitch and surge motions [29,30] have

* Corresponding author at: Department of Mechanical Science and Engineering, University of Illinois, Urbana, IL, 61801, United States of America.
E-mail address: lpchamo@illinois.edu (L.P. Chamorro).

https://doi.org/10.1016/j.apenergy.2022.118608
Received 19 August 2021; Received in revised form 29 December 2021; Accepted 22 January 2022
Available online 8 February 2022

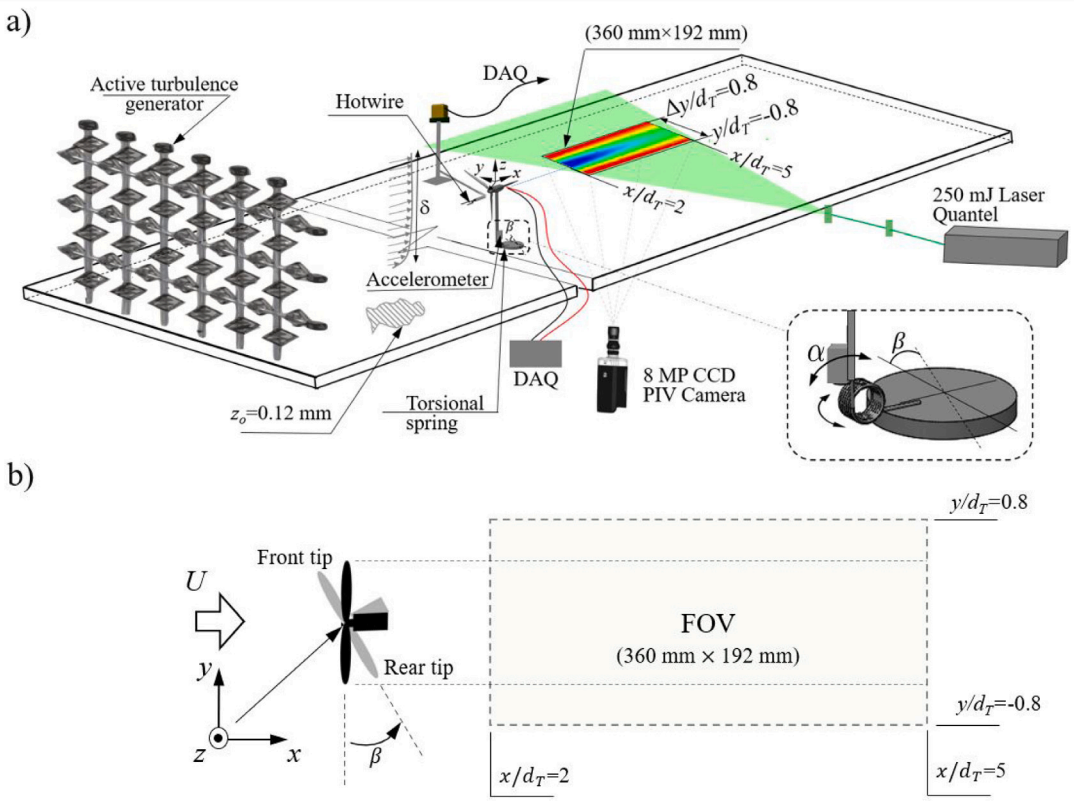

Fig. 1. (a) Basic schematic of the experimental setup illustrating the hotwire and PIV upwind and downwind of the turbine and the spring at the base of the turbine that allows tower oscillations, (b) top view.

shown asymmetric and complicated turbine wakes, which, in turn, alter the power and thrust [31]. Recently, Lei, Su, Bao, Chen, Han, and Zhou [20] explored the wake characteristics of a floating vertical axis wind turbine under platform's pitch and surge motions using numerical simulations and noted that pitch motion could alter the wake in various ways. Experimental studies [32–34] on wind turbines undergoing motions have offered valuable insights. Oguz, Clelland, Day, Incecik, Lopez, Sanchez, and Almeria [35] combined experiments and numerical simulations using FAST of the so-called Iberdrola TLP wind turbine concept under representative wind and wave conditions. They showed that numerical simulations are challenged to predict the platform response accurately. Rockel, Camp, Schmidt, Peinke, Cal, and Holling [36] performed wind tunnel experiments to characterize the influence of platform motions and compared four wake models. They noted that platform pitch induced an upward shift in the flow and departures between the model predictions and experiments. Sebastian and Lackner [37] performed multiple-DOF simulations of floating turbines; they identified various operating modes that may lead to distinct rotor-wake interactions and pointed out that aerodynamics triggered by platform motions may be significant and should be explored. Recently, Fu, Jin Zheng and Chamorro [38] studied the power output and wake fluctuations of a wind turbine undergoing a variety of forced periodic pitching and roll motions. They showed significant changes in the wake at the turbine symmetry plane and changes in the mean power output with moderate tower oscillations due to a relative gain from the cube of the relative incoming velocity impinging the rotor in the pitching and a momentum replenish in the rolling.

Despite the progress made to advance the technology and understand the impact of platform motions on the power output and related aerodynamics [39–41], the underlying physics of the problem remains obscure. Uncovering the dominant factors modulating the unsteady loading, aerodynamics, and performance of wind turbines exposed to motions, is crucial to predict the oscillations and performance of the structures and, therefore, a precursor to optimize the turbine design and operation across various flow environments and yaw misalignments. Indeed, FOWT dynamics involve the coexistence of multiple processes that pose numerous engineering challenges. Assessment of issues with reduced complexity allows gaining fundamental and practical insight. This investigation points in that direction and follows our previous work that used turbines forced to oscillate in a specific fashion [38]. Now, we have relaxed the motions of the turbines with passive oscillations and provided a base framework and a formulation towards addressing a variety of problems. The passive oscillations using carefully-selected spring stiffness provide oscillation amplitude comparable to the barge- and spar-buoy-based floating units. The tested turbine, the small oscillations, and the formulation allow understanding of the coupled interaction between flow, turbine, and oscillations. It is important to stress that much work is needed to uncover the various physics involved.

Here, we explored the power output fluctuations, wake and multi-scale oscillations of a wind turbine under various conditions experimentally and proposed models in the spectral domain for the power output and turbine motions. The experimental setup is described in Section 2, results and discussion are provided in Section 3, and main remarks are given in Section 4.

2. Experimental setup

A series of wind-tunnel experiments are performed to characterize and quantify the mean power output and the structure of the power fluctuations, wake, and motions of a model turbine able to oscillate under a turbulent boundary layer (TBL) passively.

The Eiffel-type wind tunnel of the University of Illinois at Urbana-Champaign's Renewable Energy & Turbulent Environment Group has a test section of 0.91 m wide, 0.45 m high and 6.1 m long. Details on this facility can be found in Adrian, Meinhart, and Tomkins [42]. The

ceiling is fully adjustable along the test section's span to control the pressure gradient, which is set to nearly zero during the experiments. An active turbulence generator located at the beginning of the test section induced broadband turbulence containing an inertial subrange spanning two decades. The turbulence generator has a series of vertical and horizontal rods with rectangular elements, which rotated at a frequency of 0.1 Hz using stepper motors; additional details of the turbulence generator can be found in Jin, Ji, Liu, and Chamorro [43]. Surface roughness consisting of 5 mm bulk-diameter chains was also placed every 0.2 m along the span of the test section [38] to help develop the TBL.

The model wind turbine is based on a reference model from Sandia National Laboratory [44,45]. The nacelle and blades were 3D printed with an Objet Eden 350 machine at the University of Illinois Rapid-Prototyping Lab. The turbine weight $m_1 = 0.016$ kg and the base tower weight $m_2 = 0.010$ kg resulted in a moment of inertia of $I \approx 3 \times 10^{-4}$ kg m^2. The 3-bladed rotor has a diameter of $d_T = 120$ mm, and the hub height is $z_{hub} = 120$ mm [46]. A Precision Micro-drives 112-001 Micro Core 12 mm was used as the loading system, which resulted in a rated power $P_0 \sim 1$ W. Turbine power output was measured directly from the terminals of the DC motor at 1 kHz frequency for a total sampling time $T_s = 300$ s. The power measurement had a correlation time scale of $T_c = 0.65$ s, which results in a measurement uncertainty $\sigma_E/\bar{P} = \sqrt{2T_c/T_s}\sigma_P/\bar{P} \approx 3 \times 10^{-3}$ for the zero-yaw fixed case, where σ_E, $\bar{P}$ and σ_P are the uncertainty in the mean value, measured mean power and the root mean square of the measured power fluctuations. The turbine operated at a tip-speed ratio of $\lambda = r\omega/U_{hub} \sim 5$, where ω is the angular velocity of the rotor; this is on the order of observed in utility-scale wind turbines [47]. Additional characteristics quantities of the turbine can be found in Tobin N., Hamed A.M. and Chamorro L.P.[48]. The measured power coefficient for the turbine is $C_p \sim 0.11$. This value is due to the efficiency of the generator (approximately 20% at the rotational speeds during the runs) and not indicative of the aerodynamic performance of the rotor [48]. It is worth pointing out that the model turbine can mimic the structure of power output fluctuations representative of full-scale units, as demonstrated by Tobin, Zhu, and Chamorro, [49].

The turbine was mounted over a torsional spring to allow passive oscillations. The spring stiffness was selected such that it produced moderate motions with oscillation amplitude comparable to barge- and spar-buoy-based floating wind turbines [22,50,51]; as well as the mean turbine pitch inclination of $\alpha_0 \approx 10°$ in the streamwise direction for the flow condition chosen. It was 0.27 Nm per degree in the pitch direction and ≈1.7 Nm per degree in the roll direction (henceforth base torsional spring). With this spring selection, turbine thrust coefficient C_T is estimated to be 0.62 using the wake deficit from PIV measurements, which is in line with those reported in Barone et al. [52] and Tobin et al. [53], but slightly lower than $C_T = 0.8$ indicated by Barthelmie et al. [54] for offshore wind turbines. As a complement, we also explored the effect of another torsional spring of higher stiffness, 0.32 Nm and 1.7 Nm per degree, in the streamwise and transverse directions for selected cases. The characterization of the power output, wake and turbine oscillations turbine were characterized under various yaw angles of $\beta \in [0°, 30°]$ every $\Delta\beta = 5°$. Similar characterization was performed with fixed turbines operating under the same mean inclination of 10° to aid insight into the effect of passive oscillations. A basic schematic of the setup illustrating the passive mechanism at the turbine base is shown in Fig. 1.

The mean incoming velocity at the turbine hub height was set to $U_{hub} = 8.65$ m s^{-1}, where the TBL is characterized by a friction velocity of $u_* \approx 0.55$ m s^{-1}, a roughness length $z_o \approx 0.12$ mm, and a thickness $\delta/z_{hub} \approx 2$. The velocity is inferred from hotwire anemometry within ±0.6%. The resulting Reynolds number was $Re = U_{hub}d_T/\nu \approx 7 \times 10^4$, where ν is the kinematic viscosity of air. The selected conditions allow for wake statistics with a reasonable Re independence [55,56] and were used for studying the dynamics at the array scale [57]. Fig. 2 shows

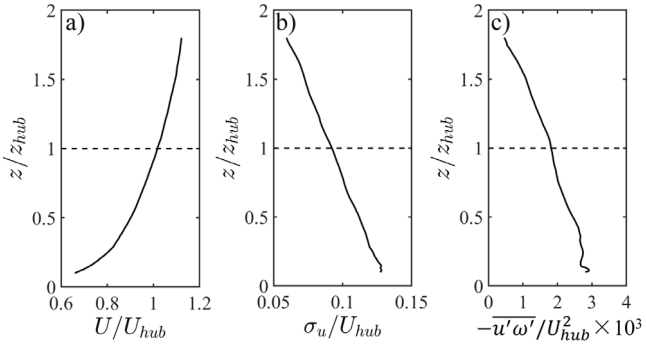

Fig. 2. Basic features of the incoming boundary layer. (a) Mean velocity U/U_{hub}, (b) turbulence intensity σ_u/U_{hub}, (c) non-dimensional, kinematic shear stress $-\overline{u'v'}/U_{hub}^2$. The horizontal, dashed lines indicate the hub height of the turbine.

non-dimensional vertical profiles of the incoming flow U/U_{hub}, turbulence intensity σ_u/U_{hub} and kinematic shear stress $-\overline{u'v'}/U_{hub}^2$; here, σ_u is the standard deviation of the streamwise velocity fluctuations.

The wind turbine's passive oscillations were tracked with a small, low-weight telemetry placed at the base at a sampling frequency of f_s = 256 Hz for periods of 90 s The sensor uses a combination of 3-axis gyroscope and 3-axis accelerometer of 16 bits and 12 bits, with uncertainties of 0.07° s^1 and 0.02 m s^2; see Hamed, Jin, and Chamorro [58] for additional details on the telemetry. The wind turbine power output was obtained at a sampling frequency of 10 kHz for periods of 120 s using a Measurement Computing USB-1608HS datalogger. It was calculated from the applied resistance and the voltage across the generators' terminals as measured with a data acquisition system (DAQ).

A planar particle image velocimetry (PIV) system from TSI was used to characterize the flow statistics of the turbine wake in a wall-parallel plane coincident with the rotor axis. The field of view (FOV) covered a region within $x/d_T \in [2, 5]$ and $y/d_T \in [-0.8, 0.8]$ (i.e., $\Delta x \times \Delta y$ = 360 mm × 192 mm), where the origin of the coordinate system was coincident with the center of the rotor. Illumination was provided by a 1 mm thick laser sheet from a 250 mJ/pulse double-pulsed laser (Quantel). Olive oil droplets of 1 μm were ejected by several Laskin nozzles placed upwind of the wind tunnel inlet to seed the flow. Two thousand image pairs at a frequency of 1 Hz were collected using an 8 MP (3320 pixels × 1560 pixels), 16 bit frame-straddle CCD camera for all the cases. The image pairs were interrogated with a recursive cross-correlation method using Insight 4G software package from TSI. The final interrogation window was 24 × 24 pixels with 50% overlap, resulting in a final vector grid spacing of $\Delta x = \Delta y = 1.4$ mm. Accounting for effects including minor camera misalignment, camera resolution, laser light sheet alignment and PIV processing, the resulted freestream velocity error had a standard deviation of $\approx 1.2 \times 10^{-2} U_{hub}$ [59–61] for the current PIV setup. Complementary hotwire (CTA mode) measurements were performed to characterize the incoming flow at the rotor axis at a high temporal resolution with frequency sampling of f = 10 kHz for measurement periods of 120 s; see additional details in Jin, Liu, Aggarwal, Singh, and Chamorro [62].

3. Results and discussion

This section discusses the impact of the turbine passive oscillations on the mean power output, structure of the power fluctuations, wake statistics and characteristics of the turbine oscillations for various yaw angles.

3.1. On the passive wind-turbine oscillations

As a step towards characterizing the effect of turbine unsteady oscillations on the power output and wake for various yawing, we

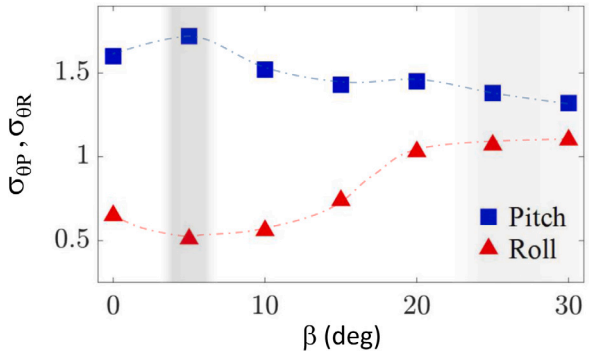

Fig. 3. Standard deviations of the turbine pitch, $\sigma_{\theta P}$, and roll, $\sigma_{\theta R}$, angles as a function of the yaw angle, β.

quantified the dominant unsteady pitch and roll motions induced by the mean flow and turbulence.

First, a bulk quantification of the turbine oscillations can be obtained with the standard deviation of the pitch ($\sigma_{\theta P}$) and roll ($\sigma_{\theta R}$) motions, which are shown in Fig. 3 for $\beta \in [0°, 30^0]$ every $\Delta\beta = 5°$. Here, the instantaneous pitch and roll angles are obtained by integrating the angular velocities inferred from the wireless sensor. The associated motions exhibited small-amplitude fluctuations around the inclination equilibrium with the maximum oscillating amplitude roughly bounded by 2°; this left a comparatively minor signature on the power output and flow recovery on the wake, as discussed later.

Promoted by the configurations studied, the pitch motion dominated the turbine dynamics. Interestingly, it was more predominant at small but non-zero yaw of $\beta \approx 5°$. The increase of yaw angle led to a gradual decrease of pitch fluctuations and an increase in roll oscillations. Such phenomenon is explored by inspecting the spectra of the angular velocity of the pitch and roll motions, $\Phi_{\dot{\alpha}}$, shown in Fig. 4 for the turbine with the two torsional springs at the base under no yaw ($\beta = 0°$) and $\beta = 30°$. The first-order natural frequency of pitch and roll motions is denoted by f_P and f_R. At a small yaw angle (Fig. 4a,c), the maximum energy occurred at $f \to f_P$, i.e., pitch motion was dominant. However, with the yaw angle increasing to $\beta = 30°$ (Fig. 4b,d), the maximum energy occurred at $f \to f_R$, indicating the comparatively high contribution of the roll motion to the energy of the fluctuations. It is worth noting that such a phenomenon occurred for the turbine with the two torsional springs.

Close inspection of the constitutive equation of the wind turbine oscillations in the spectral domain provides insight into the role of turbulence in turbine motions. The structure of the fluctuations about a fixed axis can be described by:

$$I\ddot{\alpha} = \sum_{i=1}^{n} M_i, \tag{1}$$

where I is the moment of inertia of the wind turbine, α is the angle relative to its original position, and M_i is the ith external torque. In this case, the gravity acting on the wind turbine assembly, the wind load, the restoring force from the spring, and system damping contribute to M_i. Therefore, Eq. (1) can be expressed as

$$I\ddot{\alpha} = TL + m_1 gLsin(\alpha) + \frac{1}{2}m_2 gLsin(\alpha) - k\alpha - C\dot{\alpha} \tag{2}$$

where $T = C_0 C_T \frac{1}{2}\rho A_E v^2$ is the thrust force, $C_T \approx 0.8$ is the thrust coefficient [63,64], ρ is the air density, $A_E = \pi d_T^2/4cos\beta$ is the effective swept area of the turbine rotor, m_1 is the mass of the wind turbine, m_2 is the mass of the tower, g is the acceleration of gravity, L is the tower length, k is the stiffness of torsional spring, and C is the system damping; C_0 is a characteristic parameter of the effective trust force, which is discussed next.

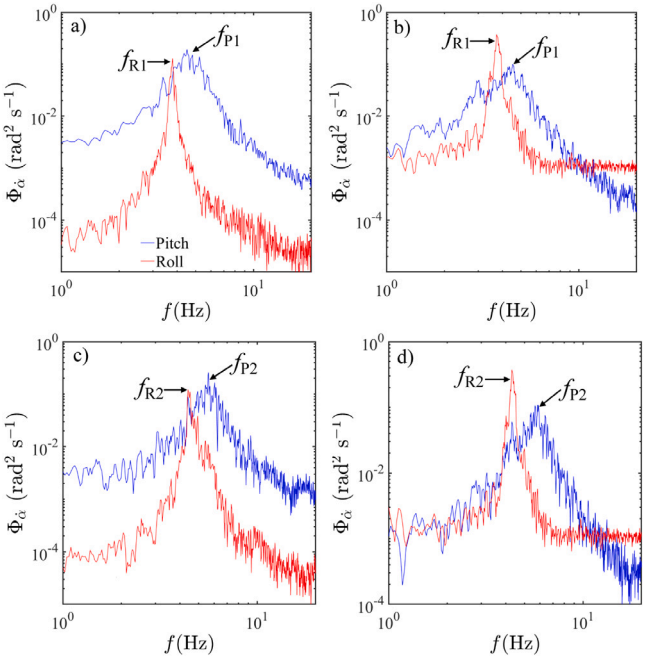

Fig. 4. Spectra of the angular velocity, $\Phi_{\dot{\alpha}}$, for the model wind turbine with the base torsional spring at yaw angles β = (a) 0° and (b) 30°. Spectra with the stiffer torsional spring at yaw angles β = (c) 0° and (d) 30°.

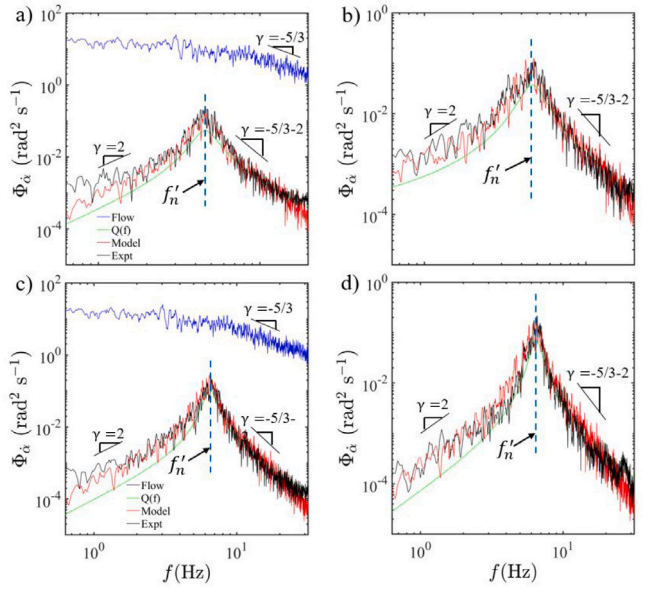

Fig. 5. Comparison of the modeled (red-colored) and measured (black-colored) spectra of the turbine oscillations $\Phi_{\dot{\alpha}}$ with the base torsional spring at yaw angles, (a) $\beta = 0°$, (b) $\beta = 30°$. Same comparison with the stiffer torsional spring at yaw angles (c) $\beta = 0°$, (d) $\beta = 30°$. The velocity spectrum of the incoming flow shown in (a) and (c) with blue color.

The Fourier transform of Eq. (2) gives:

$$\mathcal{F}(\alpha) = \frac{C_T}{I}\frac{C_0\mathcal{F}(v^2)}{k/I - (2\pi f)^2 - mgL/I + i2\pi fC/I} \tag{3}$$

Noting that $C_T = 1/2C_t\rho A_E L$, $k/I = (2\pi f_n)^2$, where f_n is the natural frequency of pitch motion, and $m = m_1 + \frac{1}{2}m_2$, then, the angular velocity fluctuations of the oscillating turbine are given by

$$\mathcal{F}(\frac{d\alpha}{dt}) = \frac{C_T}{I}\frac{2\pi i f C_0\mathcal{F}(v^2)}{(2\pi f_n)^2 - (2\pi f)^2 - mgL/I + 2\pi i fC/I} \tag{4}$$

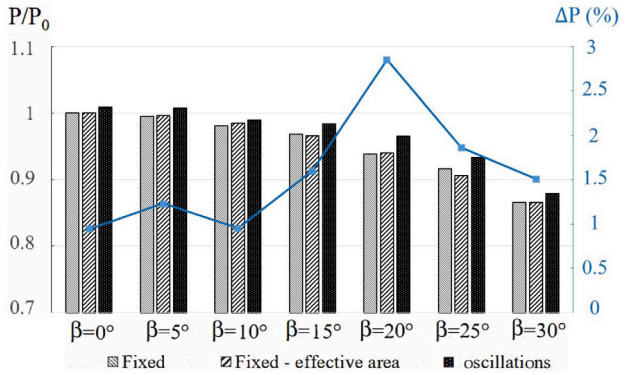

Fig. 6. Normalized power output, P/P_0, and power change $\Delta P = \frac{P_{osc}-P_{fixed}}{P_{fixed}}$, of the fixed turbines and those under small-amplitude, passive oscillations.

The turbine's angular velocity spectrum can then be written as follows:

$$\Phi_{\dot{\alpha}} = (\frac{2\pi C_T}{I})^2 \frac{{C_0}^2 f^2 \mathcal{F}(v^2)}{[(2\pi f_n')^2 - (2\pi f)^2]^2 + (\frac{2\pi C f}{I})^2} = |\mathcal{F}(v^2)|^2 Q(f) \quad (5)$$

where $f_n' = \sqrt{(f_n)^2 - \frac{mgL}{4\pi^2 I}}$ is the natural frequency of pitch motion around its inclined equilibrium, which includes the influence of gravity and spring stiffness.

The transfer function for the wind turbine oscillation is $Q(f) = (\frac{2\pi f C_T}{I})^2 {C_0}^2 \{[(2\pi f_n')^2 - (2\pi f)^2]^2 + (2\pi f C/I)^2\}^{-1}$. For $f \to 0$, $Q(f) \propto f^2$, whereas for $f \to \infty$, $Q(f) \propto f^{-2}$. It is worth pointing that for $f \to f_n$, $Q(f)$ is maximum, resulting in the well-known resonance. This corresponds to the natural frequency obtained in Fig. 4 for the two spring scenarios across β.

The coefficient C_0 is needed to estimate $\Phi_{\dot{\alpha}}$. Unlike in a fixed turbine, the turbulent energy from the incoming flow is transferred and reflected into several components of the oscillating turbines, namely, the power output fluctuations, rotor, and dynamics of the wind turbine. The bulk parameter C_0 accounts for the effective trust force that leads to the turbine pitch motions. Comparison of the modeled, based on Eq. (5), and measured spectra of the turbine pitch oscillations at various yaw angles is illustrated in Fig. 5. The incoming flow measured with hotwire is used as input for all cases shown in Fig. 5a,d. There, the transfer function $Q(f)$ is included for reference. The results indicate that $C_0 \approx 0.39$; the dynamic predicted by the proposed analytical model shows an appropriate agreement with the experimental data. It is worth noting that C_0 remains a constant across all β, indicating that the portion of energy from incoming flow fluctuation inducing the turbine pitch motion was not substantially affected by the yaw misalignment. In general, the measurements and the formulation show good agreement; the frequency and magnitude of the peak and general energy distribution are captured reasonably well. For frequencies $f > f_n$, $\Phi_{\dot{\alpha}} \propto f^{-5/3-2}$. In contrast, $\Phi_{\dot{\alpha}} \propto f^2$ in the sufficiently lower-frequency domain. Some departure in the very low-frequency region may be attributed to the limitation of the sampling frequency, and electrical noise [65]. The comparison with the turbine with the stiffer spring also showed good agreement with the formulation; there, $C_0 \approx 0.5$.

3.2. Mean power output and structure of the power fluctuations

The passive wind-turbine oscillations and yawing affected the mean and fluctuating power output. Fig. 6 summarizes the mean power output (P) of all cases normalized with that of the fixed configuration under no yaw, i.e., $\beta = 0°$ (base case with mean power output P_0).

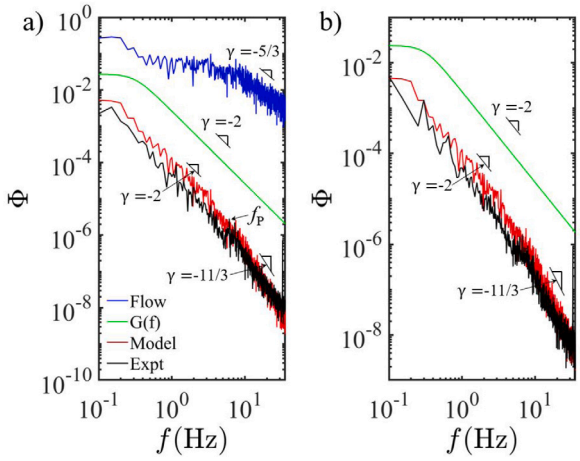

Fig. 7. Comparison of the modeled (red-colored) and measured (black-colored) power output spectra of the turbine under passive oscillations with the base torsional spring at yaw angles (a) $\beta = 0°$, (b) $\beta = 20°$. The velocity spectrum of the incoming flow is shown in (a) with blue color. Transfer function $G(f)$ (green-colored) is included for reference.

As expected, P/P_0 decreased monotonically with β in the fixed and oscillating turbines, which is more distinctive for $\beta > 15°$. The yaw reduced the effective area of the rotor. As a first-order estimation, the influence of β can be expressed as $P(\beta)/P_0 \approx \cos\beta$. As noted in Fig. 6, such estimation is reasonable. It is worth pointing out that the turbines' mean power output under passive oscillations is always slightly higher than that of the fixed counterparts across β. Fu, Jin, Zheng and Chamorro [38] reported a similar phenomenon with model turbines under forced pitch or roll motions. Note that the turbine power output is proportional to the cubic of the relative wind speed, $u_{rel} = u+u_m$, impinging on the rotor; here, u is the local incoming wind speed, and u_m is the instantaneous streamwise velocity component of turbine rotor due to oscillations. Asymmetry of the oscillations with positive u_m skewness may result in $\langle u_{rel}^3 \rangle > \langle u^3 \rangle$; here, $\langle\rangle$ denotes the time averaging operator.

The structure of the power output fluctuations of a fixed wind turbine can be illustrated via the spectral distribution ($\Phi_p(f)$). Tobin, Zhu, and Chamorro [49] derived a relation between Φ_p and the velocity spectrum of the incoming flow ($\Phi_u(f)$), which can be expressed as follows:

$$\Phi_p(f) = G(f)\Phi_u(f), \quad (6)$$

where $G(f)$ is a transfer function of the form:

$$G(f) = \frac{t_i^2}{1+(2\pi f t_i)^2}. \quad (7)$$

Here, $t_i = I\omega/(2\tau)$ is the inertial time scale, I is the inertia of the rotor, τ is the electric torque and ω (rad s^{-1}) is the rotational velocity. As a first approximation, we consider that the power spectrum of the turbine under yaw β, $\Phi_{u,\beta}(f)$ is mostly affected by the effective rotor shed area (see equation 10 in Tobin, Zhu, and Chamorro [49]) such that $\Phi_{P,\beta}(f)/\Phi_P(f) \approx cos^2(\beta)$. Despite that other effects are contributing to this spectra ratio, it provides a reasonable, simple approximation as shown now.

The spectrum of the incoming flow used as input for the scenarios shown in Fig. 7a. The incoming turbulence exhibits the well-known Kolmogorov inertial subrange $\Phi_u \propto f^{-5/3}$. The transfer function $G(f)$ is also included for reference. The spectrum of the power output from Eqs. (6) and (7) shows good agreement with all the experimental measurements. It exhibits a distinct power-law decay $\Phi \propto f^{-5/3-2}$ in the relatively high-frequency region past the onset of the inertial subrange of the incoming turbulence. Note that Eqs. (6) and (7) do not account

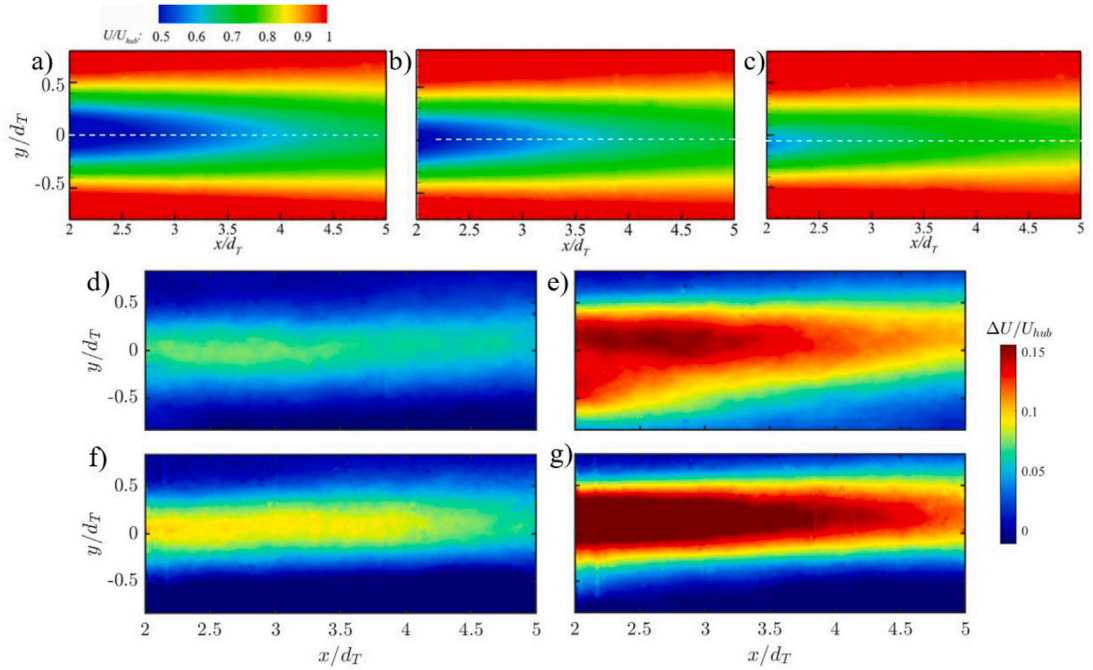

Fig. 8. Mean velocity distribution, U/U_{hub}, for the cases with the turbine under small-amplitude, passive oscillations at yaw angles (a) $\beta = 0°$, (b) $\beta = 15°$, and (c) $\beta = 30°$. Normalized velocity difference $\Delta U/U_{hub}$ between yawed and non-yawed turbines $\Delta U = U_{\beta=15°} - U_{\beta=0°}$ for the (d) fixed and (f) oscillating turbines. $\Delta U = U_{\beta=30°} - U_{\beta=0°}$ for the (e) fixed and (g) oscillating turbines.

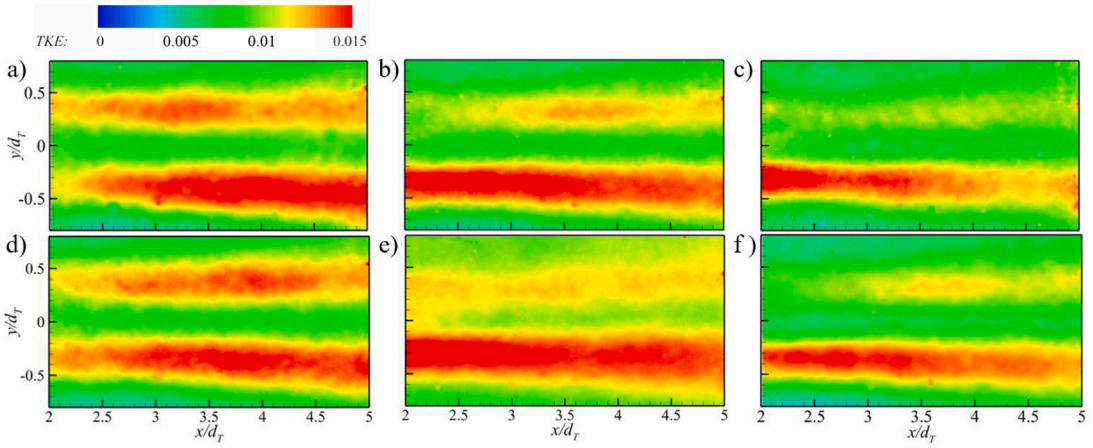

Fig. 9. In-plane turbulence kinetic energy TKE distribution for the cases with the turbine under small-amplitude, passive oscillations at yaw angles (a) $\beta = 0°$, (b) $\beta = 15°$, and (c) $\beta = 30°$, and with the fixed turbine at yaw angles (d) $\beta = 0°$, (e) $\beta = 15°$, and (f) $\beta = 30°$.

the influence of turbine motions. Indeed, the measured power spectra show a local peak (f_p in Fig. 7a) corresponding to the dominant turbine dynamic frequency discussed earlier.

3.3. On the wake statistics

The effect of the small passive oscillations of the wind turbine is assessed by comparing the wake statistics with that from the fixed turbine scenario for selected yaw configurations of $\beta = 0°$, 15° and 30°. The mean velocity distribution U/U_{hub} for the oscillating turbines are illustrated in Fig. 8a–c; the wake of the fixed turbines share similar characteristics to their oscillating counterparts, thus not shown for brevity. As expected, higher β led to reduced velocity deficit in the fixed and oscillating turbines; a similar phenomenon was discussed by, e.g., Schotter, Simon, Volker, Roar, Peinke, and Holling [66], and Qian and Ishihara [67]. The effect of oscillation is first shown by comparing velocity difference across different yaw angles β, $\Delta U = U_{\beta=15,30°} - U_{\beta=0°}$ for the fixed (Fig. 8d,e) and oscillating (Fig. 8f,g) turbines. Note a greater reduction in velocity deficit in the oscillating cases, demonstrating wake mixing enhancement and momentum injection from the incoming flow and around the rotor induced by the small-amplitude turbine oscillations. It is worth pointing out that our measurement did not show significant wake steering reported in previous work [66–69] even under relatively a high yaw angle of $\beta = 30°$. This is attributed to the high incoming turbulence level, which contributed to the wake recovery and suppression of wake deflection [67].

Bulk quantification for the wake flow fluctuations is illustrated with the in-plane turbulence kinetic energy $TKE = \langle (u'^2 + v'^2)/2U_{hub}^2 \rangle$ in Fig. 9; there, $\langle\rangle$ denotes the time averaging operator. This quantity mostly reveals the influence of yaw and turbine motions on the flow fluctuations. In general, the increase of β led to a decrease of TKE at the front tip (see Fig. 1b) for the same cases shown in Fig. 8. The reduction of the projected area of the turbine rotor facing the incoming flow with the increase of β resulted in a lower velocity deficit

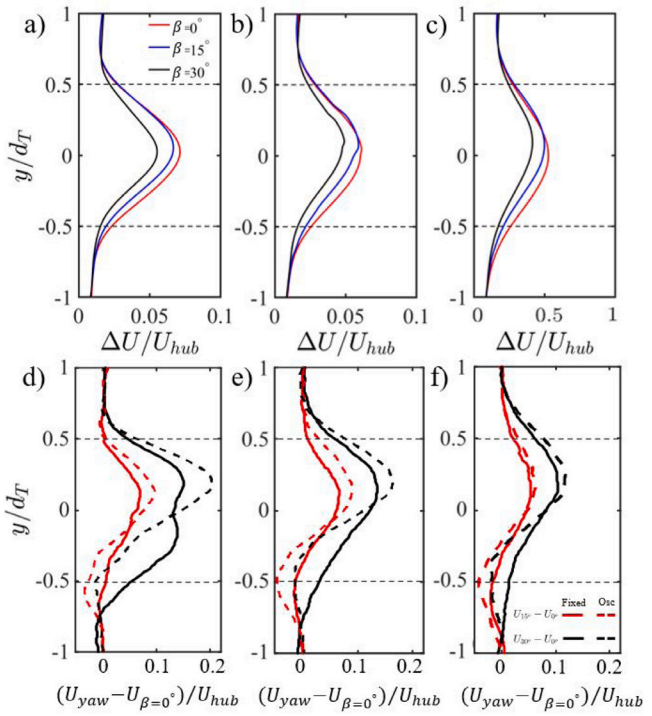

Fig. 10. Transverse velocity deficit profiles $\Delta U = U_{hub} - U(x, y, z = z_{hub})$ for various yaw angles $\beta =$ of the turbines under passive oscillations at $x/d_T = 2$, (b) 3 and (c) 4. Velocity difference between yawed and non-yawed turbines, $\Delta U = U_{\beta=15^\circ} - U_{\beta=0^\circ}$ (red) and $\Delta U = U_{\beta=30^\circ} - U_{\beta=0^\circ}$ (black), for the fixed (solid lines) and oscillating (dashed lines) turbines at $x/d_T =$ (d) 2, (e) 3 and (f) 4.

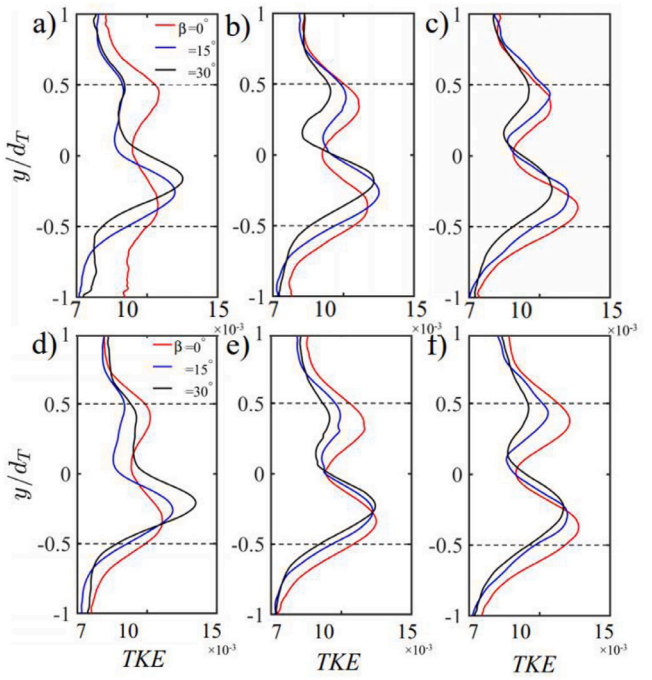

Fig. 11. Transverse profiles of the in-plane turbulence kinetic energy $TKE = \langle (u'^2 + v'^2)/2U_{hub}^2 \rangle$ for yaw angles $\beta = 0^\circ$, 15° and 30° at $x/d_T =$ (a) 2, (b) 3 and (c) 4 for the turbines under small-amplitude, passive oscillations. Cases with the fixed turbine at $x/d_T =$ (a) 2, (b) 3 and (c) 4. The horizontal, dashed lines indicate the location of the lateral tips of the fixed turbine.

(Fig. 8) and lower turbulence intensity [66,67]. It is worth noting that compared to the fixed turbine scenario, the turbine oscillations affected more the TKE distribution along the front tip side. This indicates that turbine dynamics, even under small-amplitude motions, can influence the wake fluctuations under yawing. However, such influence did not accelerate the flow recovery (Fig. 8) substantially but may impact unsteady loading on turbines placed downwind. This is a phenomenon that will be explored shortly.

Selected transverse profiles of the mean velocity and TKE distributions illustrated in Figs. 8 and 9 at $x/d_T = 2$, 3 and 4 aid to illustrate the effect of yaw and small-amplitude oscillations on the turbine wakes. Fig. 10 shows the velocity deficit $\Delta U = U_{inc} - U(y)$ and the velocity differences between yawed and non-yawed turbines normalized with that of the incoming flow at the hub height. The profiles show the wake's misalignment to the mean direction of the flow promoted by β. This misalignment increases as the wake develops downwind (Fig. 10d–f). Additionally, Fig. 10d demonstrates stronger entrainment and faster wake recovery at the wake center in the near region of the oscillating turbines; this phenomenon become weaker downwind. The TKE profiles of Fig. 11 indicate a non-negligible modulation of the small-amplitude fluctuations in the level and degree of TKE asymmetry with β. This implies that the organization of the turbulent scales changes, which is particularly important in arrays of turbines under oscillations, as indicated above.

4. Conclusions

The small-scale passive oscillation of the model wind turbine led to distinct effects on the structure dynamics, mean power output and associated fluctuations, as well as wake characteristics. The analysis is extended to a range of turbine yawing $\beta \in [0°, 30°]$.

In general, the pitch motion dominated the turbine dynamics; interestingly, it was more predominant at small but non-zero yaw of $\beta \approx 5°$. The spectral structure of the oscillations showed that the unsteady roll motions contributed substantially under high yawing. Using a fundamental relation of the turbine motions accounting for the dominant forcing and the input velocity spectrum, we derived the turbine oscillations spectrum. The formulation that shows good agreement with measurements offers insight into the structure's dynamics; it can be generalized or extended to include other type of input modulation.

The passive wind-turbine oscillations and yawing left a distinct effect on the mean and fluctuating power output. As expected, the power decreased monotonically with β in the fixed and oscillating turbines, which was more distinct for $\beta > 15°$. It is worth pointing out that the turbines' mean power output under passive oscillations is always slightly higher than that of the fixed counterparts across β. We estimated the power fluctuations structure under yaw taking into account a tuning-free formulation derived in our previous work. The power output spectrum ratio between yawed and a no-yawed turbine is taken as $cos^2(\beta)$ as a first approximation, which shows reasonable agreement.

Experiments showed that the mean velocity in the wake of the fixed and oscillating turbines exhibited minor differences for a given yawing. The small-amplitude turbine oscillation did not contribute significantly to enhancing wake mixing and momentum injection. The in-plane turbulence kinetic energy TKE revealed the influence of yaw and turbine motions on the wake's flow fluctuations. In general, the increase of β led to a decrease of TKE at the front tip. Compared to the fixed turbine scenarios, the turbine oscillations affected more the TKE distribution along the front tip side. The small-amplitude motions can influence the wake fluctuations under yawing. Despite that such influence may not accelerate the flow recovery substantially, it may impact unsteady loading on turbines placed downwind.

Finally, the study shows that small-scale, passive, unsteady turbine oscillations may produce a distinct signature on the motions, power output and wake. The spectral models derived may serve as a basic

framework to develop engineering formulations to quantify the highly complex flow–structure interactions relevant to offshore floating units. As mentioned, much work is needed to uncover the physics and the unsteady, multiscale coupling between the rotor, platform, sea and the atmospheric boundary layer involved in the dynamics of FOWT. The next step will focus on the impact of passive oscillations on the coordination and coupled operation of multiple turbines.

CRediT authorship contribution statement

Buen Zhang: Data curation, Writing – original draft, Visualization. **Yaqing Jin:** Data curation, Writing – original draft, Visualization. **Shyuan Cheng:** Data curation, Writing – original draft, Visualization. **Yuan Zheng:** Supervision, Reviewing, Funding acquisition. **Leonardo P. Chamorro:** Conceptualization, Methodology, Resources, Supervision, Writing – review & editing.

Declaration of competing interest

The authors declare that they have no known competing financial interests or personal relationships that could have appeared to influence the work reported in this paper.

Acknowledgment

This work is supported by the Mechanical Science and Engineering Department at the University of Illinois, United States of America.

References

[1] Georgilakis PS. Technical challenges associated with the integration of wind power into power systems. Renew Sustain Energy Rev 2008;12(3):852–63.
[2] Keivanpour S, Ramudhin A, Kadi Da Ait. The sustainable worldwide offshore wind energy potential: A systematic review. J Renew Sustain Enery 2017;9(6):065902.
[3] Song D, Yang J, Fan X, Liu Y, Liu A, Chen G, Young HJ. Maximum power extraction for wind turbines through a novel yaw control solution using predicted wind directions. Energy Convers Manage 2018;157:587–99.
[4] Archer Cristina L, Jacobson Mark Z. Evaluation of global wind power. J Geophys Res-Atmos 2005;110(D12).
[5] Wen T, Wang K, Cheng Z, Ong M. Spar-type vertical-axis wind turbines in moderate water depth: A feasibility study. Energies 2018;11(3):555.
[6] Breton Simon-Philippe, Moe Geir. Status, plans and technologies for offshore wind turbines in europe and north america. Renew Energy 2009;34(3):646–54.
[7] Tran Thanh Toan, Kim Dong-Hyun. A cfd study into the influence of unsteady aerodynamic interference on wind turbine surge motion. Renew Energy 2016;90:204–28.
[8] Jonkman Jason. Influence of control on the pitch damping of a floating wind turbine. In: 46th AIAA aerospace sciences meeting and exhibit. 2008, p. 1306.
[9] Namik Hazim, Stol Karl. Individual blade pitch control of floating offshore wind turbines. Wind Energy 2010;13(1):74–85.
[10] Lackner Matthew A, Rotea Mario A. Passive structural control of offshore wind turbines. Wind Energy 2011;14(3):373–88.
[11] Zuo Haoran, Bi Kaiming, Hao Hong, Li Chao. Influence of earthquake ground motion modelling on the dynamic responses of offshore wind turbines. Soil Dyn Earthq Eng 2019;121:151–67.
[12] Uzunoglu E, Soares C Guedes. Yaw motion of floating wind turbine platforms induced by pitch actuator fault in storm conditions. Renew Energy 2019;134:1056–70.
[13] Bayati I, Belloli Marco, Ferrari Davide, Fossati F, Giberti Hermes. Design of a 6-dof robotic platform for wind tunnel tests of floating wind turbines. Energy Procedia 2014;53:313–23.
[14] Liu Yuanchuan, Xiao Qing, Incecik Atilla, Peyrard Christophe. Aeroelastic analysis of a floating offshore wind turbine in platform-induced surge motion using a fully coupled cfd-mbd method. Wind Energy 2019;22(1):1–20.
[15] Tran Thanh Toan, Kim Dong-Hyun. A cfd study of coupled aerodynamic-hydrodynamic loads on a semisubmersible floating offshore wind turbine. Wind Energy 2018;21(1):70–85.
[16] Barooni M, Ale Ali N, Ashuri T. An open-source comprehensive numerical model for dynamic response and loads analysis of floating offshore wind turbines. Energy 2018;154:442–54.
[17] Kim Youngjin, Kwon Oh Joon. Effect of platform motion on aerodynamic performance and aeroelastic behavior of floating offshore wind turbine blades. Energies 2019;12(13):2519.
[18] Lee Hakjin, Lee Duck-Joo. Effects of platform motions on aerodynamic performance and unsteady wake evolution of a floating offshore wind turbine. Renew Energy 2019;143:9–23.
[19] Ruzzo Carlo, Saha Nilanjan, Arena Felice. Experimental study on heave and yaw motions of a 1: 30 spar support for offshore wind turbines. In: Proceedings of the fourth international conference in ocean engineering (ICOE2018). Springer; 2019, p. 857–68.
[20] Lei Hang, Su Jie, Bao Yan, Chen Yaoran, Han Zhaolong, Zhou Dai. Investigation of wake characteristics for the offshore floating vertical axis wind turbines in pitch and surge motions of platforms. Energy 2019;166:471–89.
[21] Tran Thanhtoan, Kim Donghyun, Song Jinseop. Computational fluid dynamic analysis of a floating offshore wind turbine experiencing platform pitching motion. Energies 2014;7(8):5011–26.
[22] Tran Thanh-Toan, Kim Dong-Hyun. The platform pitching motion of floating offshore wind turbine: A preliminary unsteady aerodynamic analysis. J Wind Eng Ind Aerodyn 2015;142:65–81.
[23] Lei Hang, Zhou Dai, Lu Jiabao, Chen Caiyong, Han Zhaolong, Bao Yan. The impact of pitch motion of a platform on the aerodynamic performance of a floating vertical axis wind turbine. Energy 2017;119:369–83.
[24] Wu Chih-Hua Keni, Nguyen Vinh-Tan. Aerodynamic simulations of offshore floating wind turbine in platform-induced pitching motion. Wind Energy 2017;20(5):835–58.
[25] Lei Hang, Zhou Dai, Bao Yan, Chen Caiyong, Ma Ning, Han Zhaolong. Numerical simulations of the unsteady aerodynamics of a floating vertical axis wind turbine in surge motion. Energy 2017;127:1–17.
[26] Wen Binrong, Tian Xinliang, Dong Xingjian, Peng Zhike, Zhang Wenming. Influences of surge motion on the power and thrust characteristics of an offshore floating wind turbine. Energy 2017;141:2054–68.
[27] Wen Binrong, Tian Xinliang, Dong Xingjian, Peng Zhike, Zhang Wenming. On the power coefficient overshoot of an offshore floating wind turbine in surge oscillations. Wind Energy 2018;21(11):1076–91.
[28] Sivalingam Krishnamoorthi, Martin Steven, Wala Abdulqadir Singapore. Numerical validation of floating offshore wind turbine scaled rotors for surge motion. Energies 2018;11(10):2578.
[29] Tran Thanh Toan, Kim Dong Hyun. The aerodynamic interference effects of a floating offshore wind turbine experiencing platform pitching and yawing motions. J Mech Sci Technol 2015;29(2):549–61.
[30] Shen Xin, Chen Jinge, Hu Ping, Zhu Xiaocheng, Du Zhaohui. Study of the unsteady aerodynamics of floating wind turbines. Energy 2018;145:793–809.
[31] Lin Lin, Wang Kai, Vassalos Dracos. Detecting wake performance of floating offshore wind turbine. Ocean Eng 2018;156:263–76.
[32] Utsunomiya Tomoaki, Sato Tomoki, Matsukuma Hidekazu, Yago Kiyokazu. Experimental validation for motion of a spar-type floating offshore wind turbine using 1/22.5 scale model. In: ASME 2009 28th international conference on ocean, offshore and arctic engineering. American Society of Mechanical Engineers; 2009, p. 951–9.
[33] Utsunomiya Tomoaki, Matsukuma Hidekazu, Minoura Shintaro, Ko Kiyohiko, Hamamura Hideki, Kobayashi Osamu, Sato Iku, Nomoto Yoshihisa, Yasui Kentaro. At sea experiment of a hybrid spar for floating offshore wind turbine using 1/10-scale model. J Offshore Mech Arct Eng 2013;135(3):034503.
[34] Li Qing'an, Kamada Yasunari, Maeda Takao, Murata Junsuke, Iida Kohei, Okumura Yuta. Fundamental study on aerodynamic force of floating offshore wind turbine with cyclic pitch mechanism. Energy 2016;99:20–31.
[35] Oguz Elif, Clelland David, Day Alexander H, Incecik Atilla, López Juan Amate, Sánchez Gustavo, Almeria Gonzalo González. Experimental and numerical analysis of a tlp floating offshore wind turbine. Ocean Eng 2018;147:591–605.
[36] Rockel Stanislav, Camp Elizabeth, Schmidt Jonas, Peinke Joachim, Cal Raúl, Hölling Michael. Experimental study on influence of pitch motion on the wake of a floating wind turbine model. Energies 2014;7(4):1954–85.
[37] Sebastian Thomas, Lackner Matthew. Analysis of the induction and wake evolution of an offshore floating wind turbine. Energies 2012;5(4):968–1000.
[38] Fu S, Jin Y, Zheng Y, Chamorro LP. Wake and power fluctuations of a model wind turbine subjected to pitch and roll oscillations. Appl Energy 2019;253:113605.
[39] Xiao Shuolin, Yang Di. Large-eddy simulation-based study of effect of swell-induced pitch motion on wake-flow statistics and power extraction of offshore wind turbines. Energies 2019;12(7):1246.
[40] Yu Youngjae, Ahn Hyeonjeong, Kim Jiyoung, Shin Hyunkyoung, et al. Effects of aerodynamic damping on motion response of a floating offshore wind turbine. In: The thirteenth ISOPE Pacific/Asia offshore mechanics symposium. International Society of Offshore and Polar Engineers; 2018.
[41] Aird Jeanie, Gaertner Evan, Lackner Matthew. Dynamic prescribed-wake vortex method for aerodynamic analysis of offshore floating wind turbines. Wind Eng 2019;43(1):47–63.
[42] Adrian Ronald J, Meinhart Carl D, Tomkins Christopher D. Vortex organization in the outer region of the turbulent boundary layer. J Fluid Mech 2000;422:1–54.
[43] Jin Y, Ji S, Liu B, Chamorro LP. On the role of thickness ratio and location of axis of rotation in the flat plate motions. J Fluids Struct 2016;64:127–37.

[44] Shiu Henry, Johnson Erick, Barone Matthew, Phillips Ryan, Straka William, Fontaine Arnold, Jonson Michael, et al. A design of a hydrofoil family for current-driven marine-hydrokinetic turbines. In: 2012 20th international conference on nuclear engineering and the ASME 2012 power conference. American Society of Mechanical Engineers; 2012, p. 839–47.
[45] Johnson E, Fontaine AA, Jonson ML, Meyer RS, Straka WA, Young S, van Dam CP, Shiu H, Barone M. A1: 8.7 scale water tunnel test of an axial flow water turbine. In: Proceedings of the 1st marine energy technology symposium, METS13. 2013, p. 10–11.
[46] Tobin Nicolas, Hamed Ali, Chamorro Leonardo. An experimental study on the effects ofwinglets on the wake and performance of a modelwind turbine. Energies 2015;8(10):11955–72.
[47] Ragheb Magdi, Ragheb Adam M. Wind turbines theory-the betz equation and optimal rotor tip speed ratio. Fund Adv Top Wind Power 2011;1(1):19–38.
[48] Tobin Nicolas, Hamed Ali M, Chamorro Leonardo P. Fractional flow speed-up from porous windbreaks for enhanced wind-turbine power. Bound-Lay Meteorol 2017;163(2):253–71.
[49] Tobin N, Zhu Hao, Chamorro LP. Spectral behaviour of the turbulence-driven power fluctuations of wind turbines. J Turbul 2015;16(9):832–46.
[50] Aboutalebi Payam, M'zoughi Fares, Garrido Izaskun, Garrido Aitor J. Performance analysis on the use of oscillating water column in barge-based floating offshore wind turbines. Mathematics 2021;9(5):475.
[51] Harriger Evan Michael. Dynamic analysis of a 5 megawatt offshore floating wind turbine. San Diego: University of California; 2011.
[52] Barone Matthew F, Johnson Erick, Fontaine Arnold A, Jonson Michael L, Meyer Richard S, Straka William A, van Dam CP, Shiu Henry. A 1: 8.7 scale water tunnel test of an axial flow water turbine. Technical report, Sandia National Laboratories; 2013.
[53] Tobin N, Zhu Hao, Chamorro LP. Spectral behaviour of the turbulence-driven power fluctuations of wind turbines. J Turbul 2015;16(9):832–46.
[54] Barthelmie RJ, Larsen GC, Frandsen ST, Folkerts L, Rados K, Pryor SC, Lange B, Schepers G. Comparison of wake model simulations with offshore wind turbine wake profiles measured by sodar. J Atmos Ocean Technol 2006;23(7):888–901.
[55] Chamorro Leonardo P, Arndt REA, Sotiropoulos Fotis. Reynolds number dependence of turbulence statistics in the wake of wind turbines. Wind Energy 2012;15(5):733–42.
[56] Sarlak H, Nishino T, Martínez-Tossas LA, Meneveau C, Sø rensen Jens Nørkær. Assessment of blockage effects on the wake characteristics and power of wind turbines. Renew Energy 2016;93:340–52.
[57] Tobin Nicolas, Chamorro Leonardo P. Turbulence coherence and its impact on wind-farm power fluctuations. J Fluid Mech 2018;855:1116–29.
[58] Hamed Ali M, Jin Yaqing, Chamorro Leonardo P. On the transient dynamics of the wake and trajectory of free falling cones with various apex angles. Exp Fluids 2015;56(11):207.
[59] Raffel Markus, Willert Christian E, Scarano Fulvio, Kähler Christian J, Wereley Steven T, Kompenhans Jürgen. Piv uncertainty and measurement accuracy. In: Particle image velocimetry. Springer; 2018, p. 203–41.
[60] Adrian Ronald J, Westerweel Jerry. Particle image velocimetry. Number 30. Cambridge University Press; 2011.
[61] Zhang Buen, Cheng Shyuan, Lu Fanghan, Zheng Yuan, Chamorro Leonardo P. Impact of topographic steps in the wake and power of a wind turbine: Part a—statistics. Energies 2020;13(23):6411.
[62] Jin Yaqing, Liu Huiwen, Aggarwal Rajan, Singh Arvind, Chamorro Leonardo. Effects of freestream turbulence in a model wind turbine wake. Energies 2016;9(10):830.
[63] Frohboese Peter, Schmuck Christian, Garrad Hassan GL. Thrust coefficients used for estimation of wake effects for fatigue load calculation. In: European wind energy conference. 2010, p. 1–10.
[64] Schaffarczyk Alois Peter. Introduction to wind turbine aerodynamics. Springer; 2014.
[65] Hobeck JD, Inman DJ. Artificial piezoelectric grass for energy harvesting from turbulence-induced vibration. Smart Mater Struct 2012;21(10):105024.
[66] Schottler Jannik, Bartl Jan Michael Simon, Mühle Franz Volker, Sætran Lars Roar, Peinke Joachim, Hölling Michael. Wind tunnel experiments on wind turbine wakes in yaw: redefining the wake width. Wind Energy Sci 2018;3:257–73.
[67] Qian Guo-Wei, Ishihara Takeshi. A new analytical wake model for yawed wind turbines. Energies 2018;11(3):665.
[68] Howland Michael F, Bossuyt Juliaan, Martínez-Tossas Luis A, Meyers Johan, Meneveau Charles. Wake structure in actuator disk models of wind turbines in yaw under uniform inflow conditions. J Renew Sustain Energy 2016;8(4):043301.
[69] Howland Michael F, Lele Sanjiva K, Dabiri John O. Wind farm power optimization through wake steering. Proc Natl Acad Sci 2019;116(29):14495–500.